ACS central science

Research Article

http://pubs.acs.org/journal/acscii

Raman Spectroscopy Reveals New Insights into the Zonal Organization of Native and Tissue-Engineered Articular Cartilage

Mads S. Bergholt,[†,‡,§,$] Jean-Philippe St-Pierre,[†,‡,§,$] Giovanni S. Offeddu,[∥] Paresh A. Parmar,[†,‡,§] Michael B. Albro,[†,‡,§] Jennifer L. Puetzer,[†,‡,§] Michelle L. Oyen,[∥] and Molly M. Stevens*[,†,‡,§]

[†]Department of Materials, Imperial College London, London SW7 2AZ, United Kingdom

[‡]Department of Bioengineering, Imperial College London, London SW7 2AZ, United Kingdom

[§]Institute of Biomedical Engineering, Imperial College London, London SW7 2AZ, United Kingdom

[∥]Nanoscience Centre, Department of Engineering, University of Cambridge, Cambridge CB3 0FF, United Kingdom

Supporting Information

ABSTRACT: Tissue architecture is intimately linked with its functions, and loss of tissue organization is often associated with pathologies. The intricate depth-dependent extracellular matrix (ECM) arrangement in articular cartilage is critical to its biomechanical functions. In this study, we developed a Raman spectroscopic imaging approach to gain new insight into the depth-dependent arrangement of native and tissue-engineered articular cartilage using bovine tissues and cells. Our results revealed previously unreported tissue complexity into at least six zones above the tidemark based on a principal component analysis and *k*-means clustering analysis of the distribution and orientation of the main ECM components. Correlation of nanoindentation and Raman spectroscopic data suggested that the biomechanics across the tissue depth are influenced by ECM microstructure rather than composition. Further, Raman spectroscopy together with multivariate analysis revealed changes in the collagen, glycosaminoglycan, and water distributions in tissue-engineered constructs over time. These changes were assessed using simple metrics that promise to instruct efforts toward the regeneration of a broad range of tissues with native zonal complexity and functional performance.

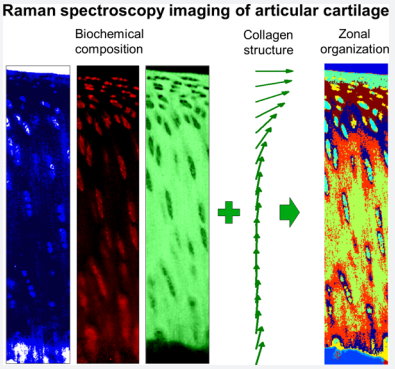

INTRODUCTION

Articular cartilage is a smooth, avascular, and aneural connective tissue that covers the surface of bones in synovial joints. This load-bearing tissue ensures low friction articulation, while also absorbing and distributing the forces transmitted through the joint to the subchondral bone.[1] The ability of articular cartilage to perform these diverse functions is directly linked to its intricate depth-dependent zonal organization.[2] It is generally accepted that the articular cartilage of skeletally mature individuals is divided into four distinct zones, namely, the superficial zone, midzone, and deep zone, as well as the zone of calcified cartilage.[3,4] Central to this model of the depth-dependent specification of articular cartilage is the organization of the collagen fibrils. The fiber alignment is parallel to the tissue surface in the superficial zone, randomly oriented in the midzone, and aligned perpendicular to the tissue surface in the deep zone.[5] However, a number of studies have fueled a debate regarding the existence of additional distinct structural regions in the most superficial zone of articular cartilage, suggesting a higher level of complexity in the zonal organization of the tissue than is generally appreciated.[6,7] Further, articular cartilage zones differ in the phenotype of resident chondrocytes,[8] the biochemical composition of the extracellular matrix (ECM),[9] and the associated mechanical properties of the tissue.

Tissue engineering approaches have provided some clinical benefits for patients suffering from articular cartilage damage or joint diseases such as osteoarthritis, notably through the development of scaffolds for improved outcome of cell-based therapies including autologous chondrocyte implantation and marrow stimulation.[10] First generation scaffold designs have mostly produced single-phase materials to support cartilage repair. However, efforts to improve long-term clinical success of tissue-engineered strategies have been increasingly focused on reproducing the zonal arrangement of native articular cartilage, toward the aim of improving the long-term outcome of these therapies.[11−13]

Histological and immunohistochemical evaluations of native and engineered articular cartilage have been instrumental in assessing the spatial distribution of major components of the ECM in cartilage tissue engineering constructs and guiding efforts to devise strategies to recreate the native tissue complexity. However, these methods remain qualitative or semiquantitative in nature, require labeling, and are not easily amenable to precise in-depth analyses of ECM component distributions.[14,15] Biochemical quantification of collagen and glycosaminoglycans (GAG) extracted from serial sections of

Received: August 10, 2016
Published: November 16, 2016

DOI: 10.1021/acscentsci.6b00222
ACS Cent. Sci. 2016, 2, 885−895

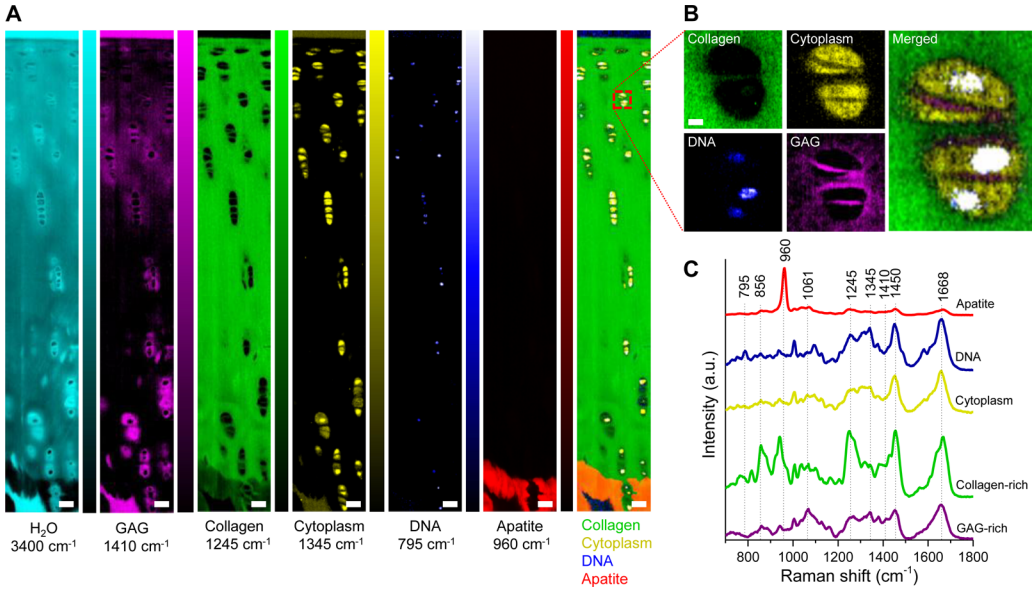

Figure 1. Raman spectroscopic imaging of articular cartilage. (A) Univariate Raman spectroscopy images of articular cartilage showing the band intensity associated with H_2O (3400 cm^{-1}), GAG (1410 cm^{-1}), collagen (1245 cm^{-1}), cytoplasm (1345 cm^{-1}), DNA (795 cm^{-1}), apatite (960 cm^{-1}), and the overlay. Scale bar: 50 μm. (B) High-resolution (~0.3 μm) Raman spectroscopy image of chondrocytes and pericellular matrix obtained by imaging the GAG (1410 cm^{-1}), cytoplasm (1345 cm^{-1}), and DNA (795 cm^{-1}) against collagen (1245 cm^{-1}). Scale bar: 3 μm. (C) Representative Raman spectra measured from articular cartilage with marked signatures for specific tissue components.

tissue has also provided insight into the depth-dependent distribution of these major ECM constituents, but is limited in the spatial resolution that can be reliably achieved.[16]

To complement findings from these approaches, several label-free optical techniques have been applied to the characterization of articular cartilage including polarized light microscopy (PLM), Fourier transform infrared (FT-IR) spectroscopy, optical coherence tomography (OCT), second harmonic generation (SHG), two photon excited fluorescence (TPEF), and Raman spectroscopy.[17−24] Raman spectroscopy is a vibrational light scattering technique that can provide a fingerprint of the biochemical composition of cells and tissues.[25] When incident laser light irradiates a sample, a small fraction of the photons (~1 in 10^8) is scattered inelastically with wavelength shifts corresponding to the Raman active normal modes of the molecules.[26] Hence, Raman spectroscopic imaging enables the extraction of a wealth of biomolecular information (i.e., specific biochemical conformation of proteins, carbohydrates, lipids, nucleic acids, etc.) in cells and tissues using endogenous biomolecules as a contrast mechanism and with submicrometer spatial resolution. Further, since Raman scattering can be described by a polarizability tensor, controlling the polarization of the incident and detected light allows structural information to be extracted.[27] Since Raman spectroscopy can be performed in aqueous environments, this technique holds key advantages over FT-IR in probing highly hydrated tissues such as articular cartilage. Raman spectroscopy has previously been used to characterize differences in the ECM of the three main zones of articular cartilage[23,24] and engineered cartilage,[28,29] but has yet to be exploited as an exploratory tool to gain insight into native tissue complexity. This could help guide the development of improved tissue engineering strategies by providing quantitative information on the composition and collagen orientation that can be compared to native tissue.

In this study, we employed Raman spectroscopy to evaluate both the spatial biochemical distribution and collagen fiber orientation across the full thickness of bovine articular cartilage. We performed an analysis of the data set without favoring accepted models of depth-dependent organization to gain new insight into the complex zonal arrangement of the tissue. Nanoindentation was used to elucidate the functional impact of the zonal arrangement of articular cartilage and the relationship between ECM composition/structure and biomechanical properties. We also elaborated an approach that harnesses Raman spectroscopic data to evaluate the depth-dependent composition of tissue-engineered cartilage constructs against that of native articular cartilage. Given mounting efforts to replicate native tissue organization with the aim of generating functional tissue-engineered constructs, this tool promises to guide efforts toward the next generation of cartilage repair/regeneration strategies. Further, the methodologies devised in this work can be adapted to enhance engineered constructs for a broad range of applications.

RESULTS AND DISCUSSION

Raman Spectroscopic Imaging of Articular Cartilage.

To gain insight into the compositional and structural properties through the depth of native articular cartilage, we first collected Raman spectra from regions spanning the entire cross section of mature bovine articular cartilage samples (n = 5 animals, 2 replicates per animal, 1000 × 400 μm maps; spatial resolution of ~1−2 μm) (Figure 1). In accordance with the literature,[23,24,30] we found Raman peaks with tentative assignments near 795 cm^{-1} (DNA), 856 cm^{-1} (proline), 875 cm^{-1} (hydroxyproline; associated with collagen), 960 cm^{-1} ($\nu_1(PO_4)$ of hydroxyapatite), 1004 cm^{-1} (ν_s(C−C) of phenylalanine), 1245 cm^{-1} (amide III ν(C−N) and δ(N−H) of collagen), 1410 cm^{-1} ($\nu_s(COO^-)$ of GAG), 1450 cm^{-1} ($\delta(CH_2)$ deformation of collagen), and 1668 cm^{-1} (amide I ν(C═O) of collagen) (for specific peak assignment see Table S1). By imaging the intensity of distinct bands centered at 3400 cm^{-1} (H_2O) (Figure S1), 1410 cm^{-1} ($\nu_s(COO^-)$ of GAG),

DOI: 10.1021/acscentsci.6b00222
ACS Cent. Sci. 2016, 2, 885−895

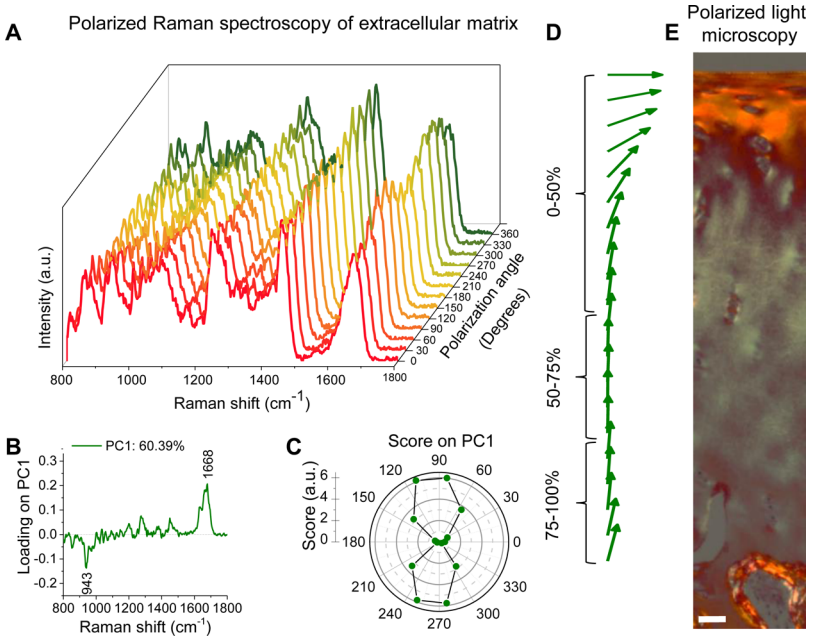

Figure 2. Collagen fiber orientation determined by Raman scattering. (A) Raman spectra of extracellular matrix (deep zone) in native articular cartilage under a full polarization rotation of the incident laser light. (B) Principal component analysis (PCA) loading (PC1: 60.39%) revealing the Raman peaks (e.g., 943 and 1668 cm^{-1}) that show the prominent anisotropic scattering. (C) Polar diagram of PC1 score for a full 360° polarization rotation showing the anisotropic response of collagen fibers in articular cartilage relative to the laser polarization. (D) Vector field derived from the empirical ratio I_{1668}/I_{943} revealing the collagen fiber orientation throughout the depth of the tissue. These have been normalized to the full tissue depth defined from the surface to the bone. (E) Polarized light microscopy (PLM) from the same sample (Picrosirius red stained histological section) showing the orientation of collagen fibers in articular cartilage. Scale bar: 50 μm.

1245 cm^{-1} (amide III of collagen), 1345 cm^{-1} (cytoplasmic biomolecules), 795 cm^{-1} (DNA), and 960 cm^{-1} ($\nu_1(PO_4)$ of hydroxyapatite), we generated false-color heat maps of the distribution of these biomolecules to enable label-free visualization of chondrocytes and the main ECM components within the native articular cartilage (Figure 1A,B). Further, we were able to identify representative Raman spectra with marked signatures for specific articular cartilage components including apatite-, DNA-, cytoplasm-, collagen-, and GAG-rich areas (Figure 1C). Since the Raman spectrum of cartilage ECM is largely dominated by the collagen signal, the weaker GAG signal can be partially masked in certain pixels (Figure 1C). With that in mind, we found that the bands near ~1410 cm^{-1} ($\nu_s(COO^-)$ of GAG provided a better contrast than the commonly used (ν_s(S═O) peak near 1061 cm^{-1}.[23] This univariate analysis of the Raman spectroscopy data allows a localization of the main components of articular cartilage, namely, collagen, GAG, water, chondrocytes, and their nuclei.

Raman spectroscopy primarily reveals compositional information about samples. However, because the laser excitation was inherently polarized at the sample in this study, using a half-waveplate we were also able to extract information on the collagen fiber orientation across the depth of articular cartilage. We found major differences in the Raman spectra of the ECM in the superficial and deep zone, emphasizing prominent changes associated with collagen Raman peaks (e.g., 856, 943, 1245, and 1668 cm^{-1}). To verify that these changes were mainly caused by the plane of alignment of the collagen fibers within the tissue relative to the laser polarization, we measured the anisotropic Raman scattering response of the deep extracellular matrix in a full 360° incident laser polarization rotation (measurements taken at 30° sample rotation intervals) (Figure 2A). This data showed a clear oscillatory behavior of the amide I band. We applied a principal component analysis (PCA) to uncover the peaks that exhibit anisotropic Raman scattering (Figure 2B,C). PC1 loading and score plots revealed strong orientation dependences relative to the laser excitation polarization, specifically at 943 cm^{-1} (CCO) and 1668 cm^{-1} (amide I ν(C═O)). We therefore used the intensity ratio I_{1668}/I_{943} as an empirical parameter that shows the collagen orientation (see Materials and Methods). Figure 2D illustrates the average collagen orientation depicted as a vector field from data of five animals (with two technical replicates). Polarized Raman spectroscopy has previously been used to evaluate the orientation of collagen fibers in tissues.[31] This Raman spectroscopy based evaluation of collagen fiber orientation is in agreement with that reported by others[5,32] and was confirmed here with polarized light microscopy (PLM) of Picrosirius red (PSR) stained sections from the same tissue (Figure 2E). We have also performed second harmonic generation (SHG) images of these tissues (Figure S2). Of note, others have reported that the collagen orientation information that can be obtained by SHG imaging of healthy articular cartilage is limited because of relatively small collagen fiber diameters compared to other tissues.[33] Hence, the use of Raman spectroscopy provides structural information that is not easily accessible with SHG in articular cartilage. The depth-dependent collagen fiber orientation in articular cartilage is the main parameter used in support of the accepted model of zonal organization of articular cartilage into superficial zone, midzone, and deep zone. Interestingly, these data showed a significant change in the average collagen fiber orientation, as measured by the intensity ratio I_{1668}/I_{943}, in the deep portion of the tissue (i.e., the depth between 75 and 100% of the total tissue thickness) compared to the 50−75% of the total tissue thickness, which exhibits perpendicular collagen orientation as

DOI: 10.1021/acscentsci.6b00222
ACS Cent. Sci. 2016, 2, 885−895

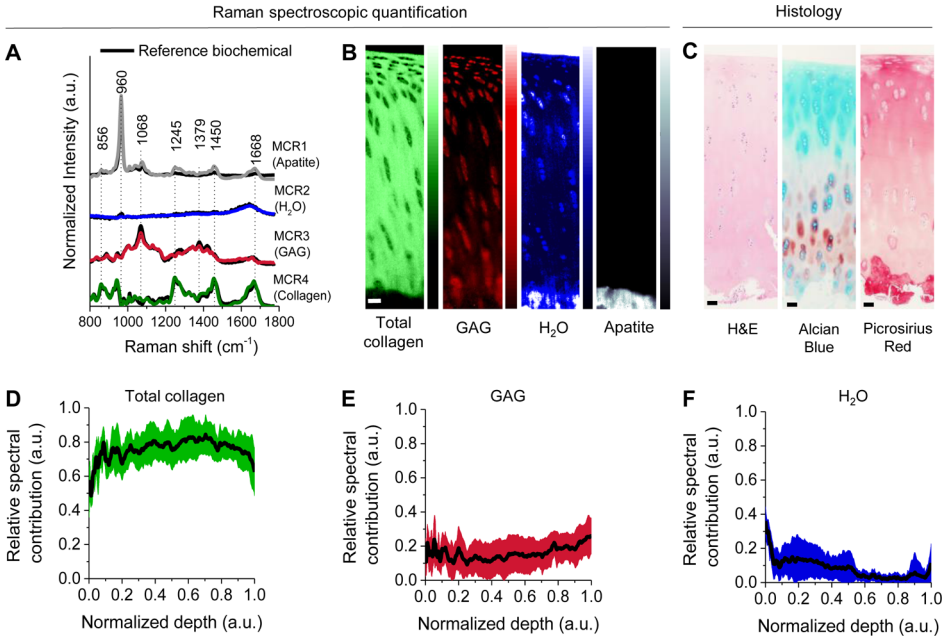

Figure 3. Relative depth-dependent biochemical distributions in native articular cartilage measured by Raman spectroscopy. (A) Raman spectra of reference biochemical (i.e., synthetic hydroxyapatite, demineralized H_2O, chondroitin sulfate, and collagen type II). Also shown are the extracted "pure" components from articular cartilage using multivariate curve resolution (MCR). The correlation coefficients were R^2 = 0.92, 0.92, 0.95 and 0.92, respectively. (B) Distribution images of collagen, GAG, H_2O, and apatite explaining a total of 89.25% of the biochemical variance in the image. The residual was associated with cellular and minor extracellular matrix biomolecules. Scale bar: 50 μm. (C) Representative hematoxylin and eosin (H&E), Alcian blue, and Picrosirius red stained histological sections of the same tissue. Scale bar: 50 μm. (D) Relative distribution of collagen, (E) GAG, and (F) H_2O in native articular cartilage across the depth of the tissue defined from the surface (0) to the calcified cartilage (1).

expected in the deeper aspect of the tissues (p < 0.001, unpaired Student's t test) (Figure 2D). These results suggest a change in the collagen network organization, with potential implications for the local mechanics of the tissue. Further evaluations using methods complementary to Raman spectroscopy will help elucidate the nature of structural changes in the collagen network occurring in the deeper aspect of the tissues.

Univariate imaging (Figure 1A) is inherently associated with uncertainty due to the superimposition of Raman peaks for different tissue biomolecules.[24] We therefore aimed to develop a robust multivariate model using multivariate curve resolution (MCR) to characterize the biochemical composition of native articular cartilage more accurately. MCR can deconvolve pure biochemical components present in the tissue spectra.[34] Figure 3A displays the Raman spectra of laboratory grade biochemicals and the four pure components extracted from the data using MCR and representing apatite (MCR1: 25.80%), water (MCR2: 4.94%), GAG (MCR3: 0.45%), and collagen (MCR4: 58.06%) accounting for a total 89.25% of the spectral variance in the Raman images. The model developed offers an excellent agreement between the deconvolved pure component spectra and the reference biochemicals: synthetic hydroxyapatite, water, chondroitin sulfate, and collagen type II (correlation coefficients R^2 of 0.92, 0.92, 0.95 and 0.92). The residual spectral variance of 10.75% was mainly associated with the chondrocyte spectral signature (i.e., cytoplasmic biomolecules and DNA) and other minor ECM biomolecules.[23] Of note, we took into account the anisotropic Raman scattering in the biochemical analysis of collagen by using the total collagen content, which was calculated as the sum of collagen fibers aligned perpendicular and parallel to the tissue surface (see Figure S3).

From the MCR data, we produced compositional maps for three of the key ECM components (i.e., collagen, GAG, and water) that illustrate their relative spatial distribution within the articular cartilage (Figure 3B). We also reconstructed the average depth-dependent distributions ± 1 standard deviation (SD) of these components for the five animals tested (Figure 3D−F). Our results indicate an increase in the relative collagen and GAG contents with tissue depth from the surface. Contrary to the relative GAG content, the relative collagen content decreases in the deeper 30% portion of articular cartilage. The relative water content is highest at the surface and decreases abruptly in the superficial aspect of the tissue and more gradually from the middle aspect. It must be emphasized that since the Raman spectra are normalized, these distributions do not report actual concentrations but rather relative amounts that reflect the contribution of the respective biomolecules to the tissue Raman spectra. It should also be noted that the distribution curves were generated without discriminating between the cellular and ECM components. The distribution profiles reported here are in agreement with observations on the biochemical content of fetal and newborn bovine articular cartilage evaluated by others using biochemical assays, but offer a much greater spatial resolution.[9] While histological evaluation enables qualitative visualization of cells, GAG, and collagen in articular cartilage (Figure 3C), the Raman spectroscopy approach developed here allows a comprehensive label-free and quantitative evaluation of both tissue composition and structure.

Raman Spectroscopy Reveals Increased Depth-Dependent Complexity of Articular Cartilage. A key advantage of using Raman spectroscopy to resolve spatial composition and organization of tissues is the wealth of data generated that can easily be harnessed in an exploratory manner

DOI: 10.1021/acscentsci.6b00222
ACS Cent. Sci. 2016, 2, 885−895

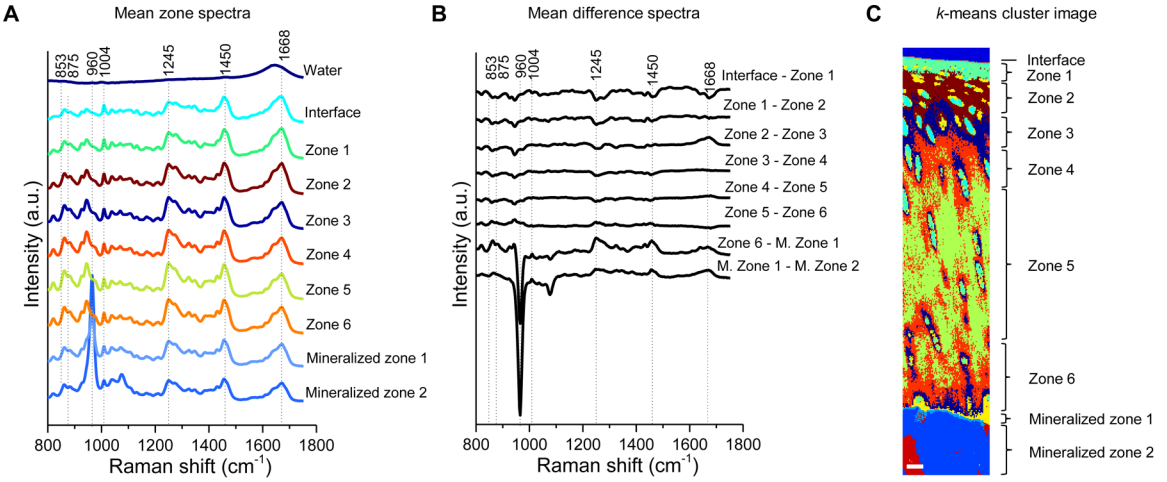

D

	Collagen	GAG	Water	Collagen orientation relative to surface (I_{1668}/I_{943})
Zone 1	+	++++	+++++	+++++
Zone 2	+++	+++	+++	++++
Zone 3	++	+++++	++	+++
Zone 4	++++	+++	+	++
Zone 5	+++++	+	+	+
Zone 6	++++	+++	+	++

Figure 4. Raman spectroscopy reveals increased complexity in the zonal organization of articular cartilage. (A) Mean Raman spectra identified for various zones identified using *k*-means clustering analysis of the normalized Raman spectra. (B) Mean difference spectra between adjacent zones. (C) Representative *k*-means cluster image of articular cartilage belonging to the individual Raman spectra. The clustering is based on both collagen fiber orientation and biochemical composition. (D) Schematics detailing the specific biochemical compositions and collagen orientation belonging to different zones. Concentrations are assigned based on the average compositions for all pixels belonging to each cluster and rescaled to the lowest and highest values. Scale bar: 50 μm.

to obtain new insight into its organization. Toward that end, we performed PCA and *k*-means clustering on the Raman spectra library generated from 10 articular cartilage samples obtained from 5 animals (see Materials and Methods). Briefly, *k*-means clustering is based on a minimization of differences within a tissue zone and a maximization of differences between tissue zones. Here, we performed sequential *k*-means clustering until further clustering stopped producing depth-dependent zones. We calculated representative mean Raman spectra corresponding to the various depth-dependent zones as well as mean difference spectra between adjacent zones (Figure 4A,B). This analysis based on both biochemical and structural (polarization-dependent signal) information contained within the spectra revealed a clear depth-dependent zonal arrangement in the tissues (Figure 4C). This clustering exercise revealed a much more complex zonal arrangement than that proposed in the literature. Based on our analysis, we report at least six distinct depth-dependent noncalcified ECM zones based on simultaneous evaluation of composition and structural information. We summarized the influence of the main ECM components (from the MCR analysis) and collagen alignment (from the univariate analysis) to each zone in Figure 4D. Because the clustering algorithm distinguished the chondrocyte areas, the depth-dependent zonal arrangement delineated here is driven by differences in the ECM only, in contrast with average distributions presented in Figure 3D−F. While some expected intra- and interanimal variation was observed including minor changes in biochemical signatures and in the thickness of each zone, the general arrangement and zonal sequence were very similar between the five animals investigated (Figure S4). The reproducibility of our results across independent animals and technical replicates suggests that the sample number used in this study is adequate. Hence, the Raman spectroscopic approach applied in this study provides novel quantifiable structural and biomolecular information without prior assumptions on the articular cartilage organization.

Nanoindentation Reveals Functional Insight into the Impact of the Zonal Arrangement of Articular Cartilage. In an effort to validate the compositional and structural findings provided by Raman spectroscopy, we performed a functional characterization of the mechanical response of articular cartilage across the depth of the tissue using nanoindentation. The latter was modeled as a poroelastic medium composed of a porous solid fraction that behaves elastically, and a liquid phase that permeates it. The time-dependent analysis performed allowed us to extract the elastic modulus E of the solid (Figure 5A), as well as its permeability to the movement of fluid within, quantified by the hydraulic permeability K (Figure 5B). Both mechanical parameters were observed to vary with depth within the tissue. Nanoindentation showed a marked increase in the elastic modulus in the deeper aspect of the tissues. As the proximity of the stiffer apatite-containing interface with articular cartilage should only impact measurements up to approximately eight times the contact radius of the nanoindenter,[35] the presence of this soft−hard tissue interface was not an important factor in the observed increase in elastic modulus across the depth of articular cartilage measured in this study. This gradual increase in elastic modulus measured in the

DOI: 10.1021/acscentsci.6b00222
ACS Cent. Sci. 2016, 2, 885−895

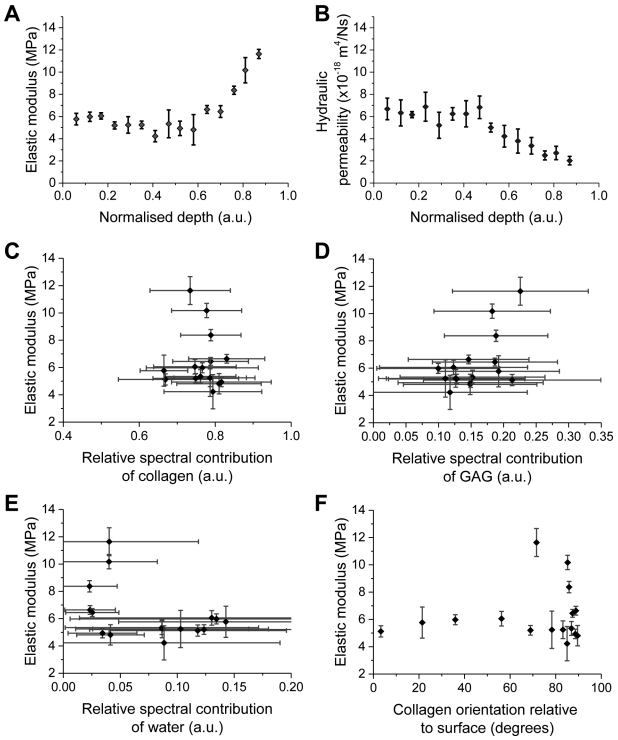

Figure 5. Nanoindentation provides functional insight into the impact of zonal arrangement in articular cartilage. (A) Elastic modulus and (B) hydraulic permeability of articular cartilage obtained by nanoindentation and mapped through the depth of the tissue. The nanoindentation data has been normalized to the full tissue depth defined from the surface (0) to the calcified cartilage (1). (C–F) Correlation of the nanoindentation data with average Raman spectroscopy MCR data on the (C) collagen concentration, (D) GAG concentration, (E) water concentration, and (F) collagen fiber orientation obtained for each nanoindentation location.

deeper aspect of articular cartilage may contribute to the mechanical integrity of the interface between hyaline and calcified cartilage along with the presence of collagen fibers that bridge this interface.[36] In contrast, the hydraulic permeability of the tissue decreased with tissue depth, suggesting that the fluid moves with greater difficulty through the porous structure. The elastic modulus of porous hydrated materials is expected to vary with the concentration of solid present in the structure.[37] However, the Raman spectroscopy compositional data did not correlate with elastic modulus values obtained from nanoindentation (Figure 5C–E). This type of behavior, whereby the elastic modulus is changing in the absence of corresponding variations in composition, has been attributed to changes in the underlying microstructure of the tissue.[38] No correlation was observed for the elastic modulus with changes in the collagen anisotropy parameter I_{1668}/I_{943}, yet data from the deeper aspect (bottom 30%) of the tissues revealed a trend toward an increased elastic modulus with increased departure from the perpendicular collagen orientation of deep zone articular cartilage (Figure S5). While further evaluations will be required to fully elucidate this observation, our data suggest that tissue microstructure (via the presence of additional structural components, cross-links, or a shift in collagen orientation), rather than composition, influences the local elastic modulus across articular cartilage depth.

Raman Spectroscopic Imaging of Tissue Engineered Cartilaginous Constructs. Given recent efforts in the field of cartilage tissue engineering to recreate the zonal organization of native tissues in an attempt to improve the functional outcome of repair constructs,[11,39,40] there is a need for methodologies to evaluate the quality of the zonal arrangement of tissue-engineered constructs in a quantifiable manner with high spatial resolution. The Raman spectroscopic imaging approach developed in this work can also be applied to instruct efforts to improve tissue-engineered cartilage constructs. To demonstrate the potential of this approach, we formed scaffold-free three-dimensional cartilage-like tissues by culturing chondrocytes isolated from full thickness bovine cartilage on porous polytetrafluoroethylene (PTFE) membranes for 2, 4, and 6 weeks according to a variation on a well-established protocol.[41−43] Cartilage-like tissues formed in this way develop a depth-dependent zonal arrangement reminiscent of native articular cartilage over time, making this an ideal model for the evaluation of the potential of Raman spectroscopy in this context.

We then measured Raman spectroscopic images of the *in vitro* formed tissues (Figure S6) (n = 3 cell extractions, 2 technical replicates per time point). As with the native tissues, we performed a MCR analysis that enabled us to extract pure Raman spectra for collagen, GAG, water, and PTFE. This data was employed to generate images (Figure 6A) that reflect ECM component distributions and are similar to those observed with typical histological staining (Figure 6B). Depth profiles of the relative contents of collagen, GAG, and water of *in vitro* formed cartilage-like tissues were also plotted (Figure 6C). To evaluate changes in depth-dependent ECM composition of *in vitro* formed cartilage and inform decisions on culture conditions toward cartilage tissue regeneration, we developed two simple and complementary metrics that enable assessments of the differences between the engineered constructs and native tissues (Figure 7). In a first metric, we evaluate the absolute area between the biochemical profiles of *in vitro* formed and native cartilage to provide insight into the differences in the depth-dependent content of collagen, GAG, and water (Figure 7A). In our model culture system, the depth-dependent GAG content significantly improved (decreased absolute integrated area) with time (one-way ANOVA, $p < 0.01$), while that of collagen did not significantly improve ($p > 0.05$). The depth profile of water content deviated from that of the native tissue after 2 weeks in culture, likely because we did not observe improvements in the collagen distribution to match those of the GAG distribution (Figure 7B). This observation was expected as engineered cartilage is often characterized by a lower collagen-to-GAG ratio than the native tissue, with an associated increase in tissue hydration. We also calculated the absolute integrated area of the area-normalized curves as a quality parameter to provide insight into the shape of the curves (Figure 7C). This parameter allows us to appreciate that the water distribution improves with culture time (Figure 7D). These results indicating some improvement in depth-dependent ECM organization are very encouraging as we selected culture conditions that did not incorporate growth factors or other biomolecules to drive the zonal arrangement in the tissue, in contrast with the work by Hayes et al. (2007) in which cellular constructs were administered frequent transforming growth factor β2.[42] Because the engineered construct spectra were dominated by the water signal, we were prevented from extracting reliable information about the collagen orientation in these tissues.

DOI: 10.1021/acscentsci.6b00222
ACS Cent. Sci. 2016, 2, 885–895

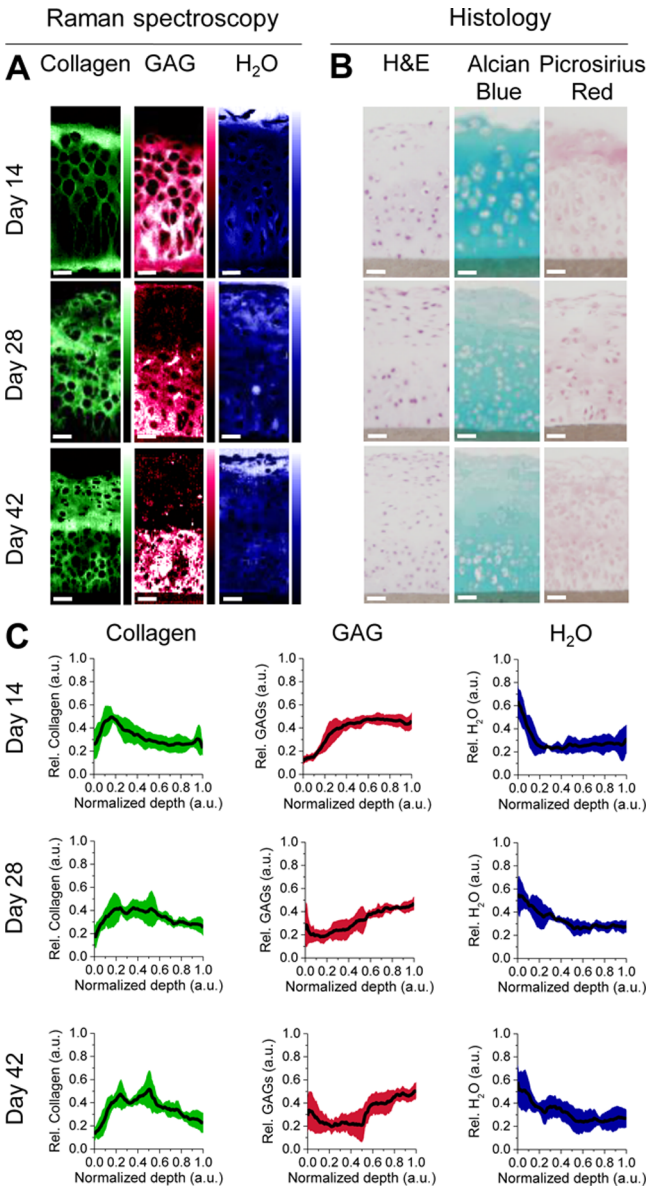

Figure 6. Depth-dependent biochemical distributions in tissue-engineered constructs measured by Raman spectroscopy. (A) Distribution images of collagen, GAG, and H_2O extracted using Raman spectroscopic imaging and MCR analysis for each incubation time (i.e., 14, 28, and 42 days). (B) Representative hematoxylin and eosin (H&E), Alcian blue, and Picrosirius red stained histological slides for each incubation time. (C) Relative distribution of collagen, GAG, and H_2O in the tissue engineered constructs for each incubation time. The data has been normalized to the tissue depth defined from the surface (0) to the calcified cartilage (1). Scale bar: 25 μm.

Further spectral analysis revealed a prominent abundance of glycogen and lipid-rich features in the cytoplasm of chondrocytes in tissue-engineered constructs (Figure S7). We did not observe these cellular signatures rich in glycogen and lipids in native articular cartilage. While the cause(s) of these cellular changes remains unidentified, it should be specified that others have observed similar appearance of glycogen and lipid droplets in an *in vivo* vitamin A induced rabbit model of osteoarthritis.[44] Suits et al. have also observed the accumulation of glycogen in chondrocyte cultures and reported that this can be influenced by culture conditions.[45]

This work on native and engineered cartilage constructs will be the basis for future pragmatic developments with the aim of applying the Raman spectroscopic approach developed herein in regenerative medicine to generate and characterize functional tissue-engineered cartilage constructs via optimized chondrogenic culture conditions toward native zonal ECM arrangement and cellular signatures. We envision that the approach developed in this study will become instrumental for biochemical and structural quality assessment of tissue-engineered constructs to repair articular cartilage.

CONCLUSIONS

In summary, Raman spectroscopy offers a novel approach to elucidate the zonal organization of articular cartilage and tissue-engineered constructs. Here, we took advantage of Raman spectroscopy to reveal increased depth-dependent compositional and structural complexity in articular cartilage. We showed that the collagen, GAG, water distributions, and collagen fibril orientation together contribute to this depth-dependent arrangement. The absence of correlation of Raman spectroscopy data with nanoindentation characterization of the tissues suggested that the tissue microstructure, rather than its composition, dictates the local elastic modulus. Further, we harnessed the quantitative nature of Raman spectroscopic data to devise metrics to guide mounting efforts in the field of cartilage tissue engineering to recreate the depth-dependent ECM arrangement that is critical to articular cartilage function. This study highlights the potential of Raman spectroscopy as an exploratory methodology in the characterization of native tissue complexity and tissue-engineered constructs. The methodology developed toward that end can be applied to the evaluation of organization in a number of tissue engineering applications.

MATERIALS AND METHODS

Osteochondral Plugs. Articular cartilage was excised as cylindrical osteochondral plugs from the metacarpal−phalangeal joint of mature cows (n = 5) aged 24 to 36 months within 48 h of death. Tissues were washed 3 times for 15 min in phosphate-buffered saline (PBS) and either frozen at −80 °C immediately (for nanoindentation) or fixed in 4% (v/v) paraformaldehyde in PBS for 30 min before being stored at 4 °C in PBS until use (for Raman spectroscopic imaging and histology). A comparison of unfixed and prefixed tissue samples was performed to demonstrate that fixation did not considerably affect Raman spectra of articular cartilage. Fixation was thus used to allow repeated measurements on the same samples over time if needed.

Chondrocyte Isolation. Articular cartilage was excised aseptically from the full thickness of metacarpal−phalangeal joints of mature cows (n = 3) aged 24 to 36 months within 48 h of death. Chondrocytes were isolated from the tissue by sequential enzymatic digestion at 37 °C (0.2% (w/v) Pronase (Roche Applied Science) in Dulbecco's modified Eagle's medium (DMEM; 4.5 g/L glucose; Invitrogen) for 1 h followed by 0.04% (w/v) collagenase type I (Sigma) in DMEM overnight).

Substrates. Hydrophilic polytetrafluoroethylene (PTFE) membranes (Millipore) encased in a cell chamber were incubated with 0.5 mg/mL collagen type II (Sigma-Aldrich) in 0.1 N acetic acid overnight to allow full evaporation of the solution. The inserts were then washed 3 times in PBS before cell seeding.

DOI: 10.1021/acscentsci.6b00222
ACS Cent. Sci. 2016, 2, 885−895

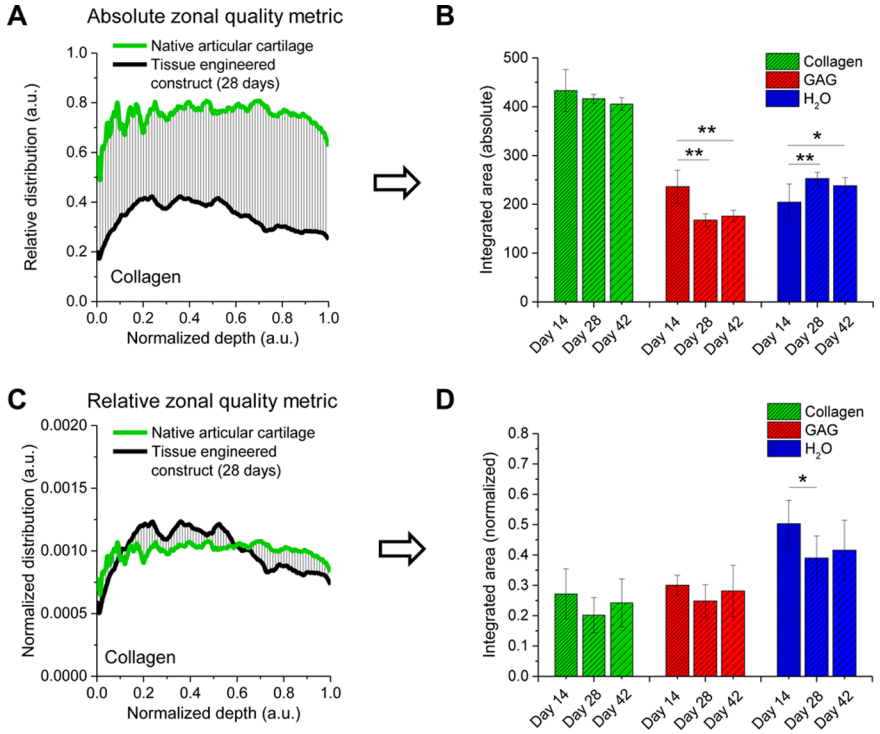

Figure 7. Metrics to evaluate the evolution of zonal organization in tissue engineered constructs. (A) The absolute zonal quality metric defined as the absolute area between the curves for the native cartilage and *in vitro* formed cartilaginous constructs at each harvesting time point. The example tissue construct curve shown is that for tissues harvested at day 28. (B) Mean absolute zonal quality metric ± standard deviation (SD) measured at various culture times. (C) The relative zonal quality metric defined as the absolute integrated area of area normalized curves between native cartilage and the cartilaginous constructs revealing differences in the shape of the biochemical distributions. The example tissue construct curve shown is that for tissues harvested at day 28. (D) Mean relative zonal quality metric ± SD measured at various time points. All curves have been normalized to the tissue depth defined from the surface (0) to the PTFE (1). Statistical significance was defined by one-way analysis of variance (ANOVA) with *post hoc* least significant differences (LSD) test, $*p < 0.05$ $**p < 0.01$, $n = 3$ cell extractions.

Tissue-Engineered Constructs. The cell chambers were placed in 24 well plates, and 750 μL of DMEM supplemented with 5% (v/v) fetal bovine serum (HyClone) was added to each well outside the cell chamber. The isolated chondrocytes were seeded on top of membrane inserts (1×10^6 cells in 750 μL per membrane; 12 mm diameter) in DMEM supplemented with 5% (v/v) fetal bovine serum and incubated at 37 °C in an atmosphere characterized by 95% relative humidity and 5% CO_2. On day 2, the medium was supplemented with ascorbic acid (50 μg/mL; Sigma-Aldrich) and the FBS supplementation was increased to 10% (v/v). The culture medium was changed every 2−3 days. Cultures were harvested at 14, 28, and 42 days. As for native articular cartilage, the *in vitro* cultured cartilage-like tissues were washed 3 times for 15 min in PBS, and fixed in 4% (v/v) paraformaldehyde for 30 min.

Histological Evaluation. The native and *in vitro* cultured cartilage were divided into two halves. The portion for Raman spectroscopic imaging was stored at 4 °C in PBS until used, and the portion for histology was embedded in paraffin, sectioned at a thickness of 4 μm, and mounted on treated slides (Superfrost Plus, Thermo Scientific). Sections were dewaxed for 5 min in xylene and hydrated through an ethanol to distilled water series. Slides were stained with hematoxylin and eosin (H&E) for cell nuclei and matrix, Alcian blue (AB; pH 2.5) for sulfated GAG, and Picrosirius red (PSR) for collagen, and then imaged using an Olympus BX51 microscope equipped with an Olympus DP70 camera. Polarized light microscopy was performed on PSR stained sections using the same microscope.

Second Harmonic Generation Imaging. Second harmonic generation (SHG) imaging was performed on fixed full thickness osteochondral plugs from mature cows. Samples were either cut perpendicular to the surface and imaged submerged in PBS or embedded into paraffin blocks, sectioned, and stained with Picrosirius red. Imaging was performed on a Leica SP5 inverted confocal microscope equipped with multiple lasers, including a 488 nm and a multiphoton laser. The multiphoton laser was a Newport Spectra-Physics Two Photon Laser (Mai Tai DeepSee 3074) capable of being tuned from 690 to 1020 nm and generating a pulse equal to or less than 100 fs. The Mai Tai laser was tuned to 890 nm wavelength to produce a SHG signal from type II collagen collected at 435−455 nm, while the 488 nm laser was used to excite autofluorescence of chondrocytes collected at 491−616 nm. All images were obtained at a scan speed of 400 Hz using a HCX PL APO CS 40× 1.25−0.5 oil objective. Noise was reduced by collecting images at 1024 × 1024 pixels with a line average of 4, and the signal was intensified by accumulating 4 frames per image.

Sample Preparation for Raman Spectroscopic Imaging. The tissues were cemented onto a polystyrene surface using a small quantity of cyanoacrylate so as to expose their cross section. They were then immersed in a drop of PBS and frozen on a cryosectioning block. Using a cryostat (Bright Instruments Ltd.), the tissues were sectioned flat at a 45° angle relative to the articular surface to ensure that the zonal organization observed was not an artifact of sectioning. Once a flat tissue cross section was obtained relative to the polystyrene surface, the samples were stored at 4 °C in PBS until Raman

DOI: 10.1021/acscentsci.6b00222
ACS Cent. Sci. 2016, 2, 885−895

spectroscopic imaging was performed. Tissue cross-section samples imaged by Raman spectroscopy were prepared to a thickness of more than 1 mm.

Raman Spectroscopic Imaging. The confocal Raman microspectroscopy system used for imaging of native cartilage and tissue-engineered constructs consists of an upright microscope (Alpha 3000, WITec, GmbH) equipped with a piezoelectric stage. A green laser (λ_{ex} = 532 nm, WITec, GmbH) with a maximum output of 75 mW was fiber-coupled into the microscope using a low OH single mode polarization preserving silica fiber. The excitation laser light had a polarization ratio of 1:100 at the sample. The measurements in this study can be regarded as unpolarized because no polarization analyzer was used. All Raman images were measured using a Leica 63×/0.75 water immersion objective. Using a 50 μm ultralow OH silica fiber acting as a confocal pinhole, the backscattered Raman signals were fed into a high-throughput imaging spectrograph (UHTS 300, WITec, GmbH) with a 600 groove/mm grating, equipped with a thermoelectrically cooled (−60 °C), charge-coupled device (CCD) camera (Newton, Andor Technology Ltd.). The system acquires Raman spectra in the range from 0 to 3700 cm^{-1} with a spectral resolution of ∼11 cm^{-1}. The atomic emission lines of the argon/mercury spectral calibration lamp (HG-1, Ocean Optics, Inc.) were used for calibration of the wavelength axis. Pixelation noise in the Raman images was reduced using linear interpolation.

Collagen Fiber Anisotropy Measurements. Polarized confocal Raman spectra (n = 13) of native articular cartilage were measured from the deep zone in a full 360° rotation (30° intervals) of the incident laser light using a half-waveplate. Each Raman spectrum was collected with an acquisition time of 5 s, 1 accumulation, and a power on the sample of ∼41 mW using the 532 nm laser excitation. Principal component analysis (PCA) was applied to extract the anisotropic spectral variation from the biological Raman spectra. The ratio of the peaks that showed highest anisotropic scattering (i.e., 943 cm^{-1} (CCO) and 1668 cm^{-1} (amide I)) was used to estimate the collagen orientation. We calculated an empirical metric to represent the average collagen orientation through the depth of the tissue using the intensity ratio I_{1668}/I_{943}. These values were first rescaled to one and normalized over the entire depth of the tissues. In this way an intensity ratio of one was associated with the alignment of collagen parallel to the surface, while an intensity ratio of zero was associated with perpendicular alignment. The average collagen fiber orientation angles were then calculated using arctan of the rescaled intensity ratio at 20 data points throughout the tissue depth. We report the average orientation combining the data from all 5 animals with two technical replicates.

Raman Spectroscopy of Tissues and Pure Biochemical Components. Raman images (∼1000 × 400 μm (spatial resolution of ∼2 μm)) of native articular cartilage and tissue engineered constructs were measured by continuous scanning. Each Raman spectrum was collected with an acquisition time of 0.3−0.5 s, 1 accumulation, and a power on the sample of ∼41 mW using the 532 nm laser excitation. No sample degradation was noticed using this power density. For comparison, reference Raman spectra were also measured of chondroitin sulfate (Sigma-Aldrich), collagen type II (Sigma-Aldrich), synthetic hydroxyapatite (Sigma-Aldrich), 1,2-dioleoyl-*sn*-glycero-3-phosphocholine (DOPC) (Sigma-Aldrich), glycogen (Sigma-Aldrich), and demineralized H_2O using similar experimental parameters.

Multivariate Statistical Analysis. Spectral analysis was performed in the fingerprint range (700−1800 cm^{-1}) due to its higher molecular specificity. Before multivariate statistical analysis, the Raman spectra were preprocessed using well-established techniques. First, to remove tissue autofluorescence, a constrained second-order polynomial was found optimum and fitted to the raw spectrum in the range 700−3600 cm^{-1}, and this polynomial was then subtracted to produce the Raman spectrum alone (this was done in Control Four, Witec, GmbH). The extracted Raman spectrum was then vector normalized to reduce confounding factors such as tissue optical properties, focusing effects, collection efficiencies, and power density variations. All Raman images were combined into a single large data set and analyzed together using non-negativity constrained multivariate curve resolution (MCR). Raman spectral outliers due to cosmic rays were identified and excluded from the model using Q-residuals. MCR produces pseudo pure components without requiring prior information.[34] For native tissue a model complexity of five components was chosen essentially representing collagen aligned perpendicular and parallel to the articulating surface, GAG, H_2O, and calcium phosphate based mineral. To account for the anisotropic Raman scattering in the biochemical analysis of collagen, the total collagen content was calculated as the sum of collagen aligned perpendicular and parallel to the articulating surface. The mean abundance profiles ± 1 standard deviation (SD) extracted using MCR were compared by normalizing to the sum of total collagen, GAG, and H_2O and normalizing the distance from the articular surface to the depth of the presence of the $\nu_1(PO_4)$ calcium phosphate peak at 960 cm^{-1} or for tissue engineered constructs, polytetrafluoroethylene at 732 cm^{-1}. Multivariate statistical analysis and clustering analysis were performed using PLS_Toolbox (Eigenvector Research, Manson, WA) and in-house written scripts in the Matlab 2014b (Mathworks, Natick, MA) programing environment on a Linux Ubuntu v15.04 multicore server (12 core, i7 3.3 Ghz processors, 64 Gb memory). Univariate peak imaging was done in Control Four (WITec, GmbH).

Clustering Analysis of Zonal Organization. The preprocessed normalized spectra were compressed using a three component PCA and fed to a k-means clustering analysis to uncover the zonal organization in cartilage across the series of Raman images. It should be noted that the biochemical gradients, in principle, will give rise to a continuum of clusters. To ensure that the zones identified were genuine, we performed k-means with various numbers of clusters (with 5 replicates to search for global minima). We chose the maximum number of clusters that still gave rise to depth-dependent clustering of the ECM. Any clustering related to chondrocytes was not included in the evaluation.

Nanoindentation. The time-dependent mechanical response of articular cartilage as a result of depth within the tissue was determined by means of displacement-control nanoindentation on a Hysitron Ubi-1 Nanoindenter (Hysitron, USA). A diamond spherical indenter with a radius of 50 μm was used for this purpose at an indentation depth of 1 μm. The small indentation depth generates an effective contact radius of approximately 7 μm. The ramp-hold profile involved a ramp time of 5 s, followed by a hold of 20 s within which a force plateau was reached. Tests were performed at room temperature on n = 3 hydrated specimens, each representative of a

DOI: 10.1021/acscentsci.6b00222
ACS Cent. Sci. 2016, 2, 885−895

distinct animal. Three line scans consisting of 15 separate indents were performed on each sample, for a total of nine scans and 135 indents. Algorithms based on exponential curve fitting of the load−time profile in a poroelastic framework were used for the analysis, which yielded values for the drained elastic modulus E, and the hydraulic permeability K of the tissues.[35]

Statistical Analysis. Statistical significance for two group comparisons was calculated using Student's t test. $p < 0.05$ was considered statistically significant. Prior to testing for equal variance using Levene's test the data was transformed to logarithmic scale. Statistical significance for multiple comparisons was calculated using one-way analysis of variance (ANOVA) with *post hoc* least significant differences (LSD) test. $p < 0.05$ was considered to be statistically significant. All statistical analysis was performed using Origin Pro 9.1 (OriginLab, Northampton, MA).

■ ASSOCIATED CONTENT

Supporting Information

The Supporting Information is available free of charge on the ACS Publications website at DOI: 10.1021/acscentsci.6b00222.

The raw research data supporting this publication is available online at http://doi.org/10.5281/zenodo.163327. Table S1 and Figures S1−S7 (PDF)

■ AUTHOR INFORMATION

Corresponding Author

*E-mail: m.stevens@imperial.ac.uk.

Author Contributions

M.S.B. and J.-P.S.-P. contributed equally to the work. M.S.B. and J.-P.S.-P. designed the study, interpreted the data, and wrote the paper. M.S.B. conducted Raman spectroscopy work and data analyses. J.-P.S.-P. performed sample preparation and cultured tissue engineered constructs. G.S.O. performed nanoindentation, conducted nanoindentation data analysis, and helped write the manuscript. P.A.P. conducted sample preparation and histological evaluations. M.B.A. contributed to scientific discussions and helped interpret the data. J.L.P. conducted second harmonic generation imaging. M.L.O. and M.M.S. contributed to the study design, scientific discussions, data interpretation, and the manuscript. M.M.S. supervised the study.

Author Contributions

$These authors contributed equally to the work.

Notes

The authors declare no competing financial interest.

■ ACKNOWLEDGMENTS

M.S.B., J.-P.S.-P., and M.M.S. acknowledge the support of the Medical Research Council, the Engineering and Physical Sciences Research Council, and the Biotechnology and Biological Sciences Research Council UK Regenerative Medicine Platform Hubs "Acellular Approaches for Therapeutic Delivery" (MR/K026682/1) and "A Hub for Engineering and Exploiting the Stem Cell Niche" (MR/K026666/1). J.-P.S.-P. and M.M.S. were also supported by the Medical Engineering Solutions in the Osteoarthritis Centre of Excellence, funded by the Wellcome Trust and the Engineering and Physical Sciences Research Council (088844). J.-P.S.-P. would like to acknowledge the Value in People Award from the Wellcome Trust Institutional Strategic Support Fund (097816/Z/11/A). M.M.S. also acknowledges the support from the ERC Seventh Framework Programme Consolidator grant "Naturale CG" under Grant Agreement No. 616417. G.S.O. and M.L.O. are thankful for the support of the Nano Doctoral Training Centre (NanoDTC), University of Cambridge, and the EPSRC (EP/G037221/1). Finally, the authors would like to thank Lorraine Lawrence for the preparation of histological sections.

■ REFERENCES

(1) Poole, C. A.; Flint, M. H.; Beaumont, B. W. Morphological and functional interrelationships of articular cartilage matrices. *J. Anat.* **1984**, *138*, 113−138.

(2) Huber, M.; Trattnig, S.; Lintner, F. Anatomy, Biochemistry, and Physiology of Articular Cartilage. *Invest. Radiol.* **2000**, *35*, 573−580.

(3) Decker, R.; Koyama, E.; Pacifici, M. Articular Cartilage: Structural and Developmental Intricacies and Questions. *Curr. Osteoporos. Rep.* **2015**, *13*, 407−414.

(4) Wong, M.; Carter, D. R. Articular cartilage functional histomorphology and mechanobiology: a research perspective. *Bone* **2003**, *33*, 1−13.

(5) Jeffery, A. K.; Blunn, G. W.; Archer, C. W.; Bentley, G. Three-dimensional collagen architecture in bovine articular cartilage. *J. Bone Joint Surg. Br.* **1991**, *73*, 795−801.

(6) Fujioka, R.; Aoyama, T.; Takakuwa, T. The layered structure of the articular surface. *Osteoarthr. Cartilage* **2013**, *21*, 1092−1098.

(7) MacConaill, M. A. The movements of bones and joints. *J. Bone Joint Surg. Br.* **1951**, *33-B*, 251−257.

(8) Poole, A. R.; Kojima, T.; Yasuda, T.; Mwale, F.; Kobayashi, M.; Laverty, S. Composition and structure of articular cartilage: a template for tissue repair. *Clin. Orthop. Relat. Res.* **2001**, *391*, S26−33.

(9) Klein, T. J.; Chaudhry, M.; Bae, W. C.; Sah, R. L. Depth-dependent biomechanical and biochemical properties of fetal, newborn, and tissue-engineered articular cartilage. *J. Biomech.* **2007**, *40*, 182−190.

(10) Hunziker, E. B.; Lippuner, K.; Keel, M. J.; Shintani, N. An educational review of cartilage repair: precepts & practice–myths & misconceptions–progress & prospects. *Osteoarthr. Cartilage* **2015**, *23*, 334−350.

(11) Steele, J. A.; McCullen, S. D.; Callanan, A.; Autefage, H.; Accardi, M. A.; Dini, D.; Stevens, M. M. Combinatorial scaffold morphologies for zonal articular cartilage engineering. *Acta Biomater.* **2014**, *10*, 2065−2075.

(12) Arora, A.; Kothari, A.; Katti, D. S. Pore orientation mediated control of mechanical behavior of scaffolds and its application in cartilage-mimetic scaffold design. *J. Mech. Behav. Biomed. Mater.* **2015**, *51*, 169−183.

(13) McCullen, S. D.; Autefage, H.; Callanan, A.; Gentleman, E.; Stevens, M. M. Anisotropic fibrous scaffolds for articular cartilage regeneration. *Tissue Eng., Part A* **2012**, *18*, 2073−2083.

(14) Hillman, H. Limitations of clinical and biological histology. *Med. Hypotheses* **2000**, *54*, 553−564.

(15) Camplejohn, K. L.; Allard, S. A. Limitations of safranin 'O' staining in proteoglycan-depleted cartilage demonstrated with monoclonal antibodies. *Histochemistry* **1988**, *89*, 185−188.

(16) Albro, M. B.; Nims, R. J.; Durney, K. M.; Cigan, A. D.; Shim, J. J.; Vunjak-Novakovic, G.; Hung, C. T.; Ateshian, G. A. Heterogeneous engineered cartilage growth results from gradients of media-supplemented active TGF-β and is ameliorated by the alternative supplementation of latent TGF-β. *Biomaterials* **2016**, *77*, 173−185.

(17) Mansfield, J.; Moger, J.; Green, E.; Moger, C.; Winlove, C. P. Chemically specific imaging and in-situ chemical analysis of articular cartilage with stimulated Raman scattering. *J. Biophotonics* **2013**, *6*, 803−814.

(18) Mansfield, J.; Yu, J.; Attenburrow, D.; Moger, J.; Tirlapur, U.; Urban, J.; Cui, Z.; Winlove, P. The elastin network: its relationship with collagen and cells in articular cartilage as visualized by multiphoton microscopy. *J. Anat.* **2009**, *215*, 682−691.

DOI: 10.1021/acscentsci.6b00222
ACS Cent. Sci. 2016, 2, 885−895

(19) Xia, Y.; Moody, J. B.; Burton-Wurster, N.; Lust, G. Quantitative in situ correlation between microscopic MRI and polarized light microscopy studies of articular cartilage. *Osteoarthr. Cartilage* **2001**, *9*, 393−406.
(20) Herrmann, J. M.; Pitris, C.; Bouma, B. E.; Boppart, S. A.; Jesser, C. A.; Stamper, D. L.; Fujimoto, J. G.; Brezinski, M. E. High resolution imaging of normal and osteoarthritic cartilage with optical coherence tomography. *J. Rheumatol.* **1999**, *26*, 627−635.
(21) Camacho, N. P.; West, P.; Torzilli, P. A.; Mendelsohn, R. FTIR microscopic imaging of collagen and proteoglycan in bovine cartilage. *Biopolymers* **2001**, *62*, 1−8.
(22) Lu, F. K.; Basu, S.; Igras, V.; Hoang, M. P.; Ji, M.; Fu, D.; Holtom, G. R.; Neel, V. A.; Freudiger, C. W.; Fisher, D. E.; Xie, X. S. Label-free DNA imaging in vivo with stimulated Raman scattering microscopy. *Proc. Natl. Acad. Sci. U. S. A.* **2015**, *112*, 11624−11629.
(23) Gamsjaeger, S.; Klaushofer, K.; Paschalis, E. P. Raman analysis of proteoglycans simultaneously in bone and cartilage. *J. Raman Spectrosc.* **2014**, *45*, 794−800.
(24) Bonifacio, A.; Beleites, C.; Vittur, F.; Marsich, E.; Semeraro, S.; Paoletti, S.; Sergo, V. Chemical imaging of articular cartilage sections with Raman mapping, employing uni- and multi-variate methods for data analysis. *Analyst* **2010**, *135*, 3193−3204.
(25) Puppels, G. J.; de Mul, F. F. M.; Otto, C.; Greve, J.; Robert-Nicoud, M.; Arndt-Jovin, D. J.; Jovin, T. M. Studying single living cells and chromosomes by confocal Raman microspectroscopy. *Nature* **1990**, *347*, 301−303.
(26) Raman, C. V.; Krishnan, K. S. A New Type of Secondary Radiation. *Nature* **1928**, *121*, 501−502.
(27) Tsuboi, M.; Thomas, G. J. Raman Scattering Tensors in Biological Molecules and Their Assemblies. *Appl. Spectrosc. Rev.* **1997**, *32*, 263−299.
(28) Kunstar, A.; Leferink, A. M.; Okagbare, P. I.; Morris, M. D.; Roessler, B. J.; Otto, C.; Karperien, M.; van Blitterswijk, C. A.; Moroni, L.; van Apeldoorn, A. A. Label-free Raman monitoring of extracellular matrix formation in three-dimensional polymeric scaffolds. *J. R. Soc., Interface* **2013**, *10*, 20130464−20130464.
(29) Kunstar, A.; Otto, C.; Karperien, M.; van Blitterswijk, C.; van Apeldoorn, A. Raman microspectroscopy: a noninvasive analysis tool for monitoring of collagen-containing extracellular matrix formation in a medium-throughput culture system. *Tissue Eng., Part C* **2011**, *17*, 737−744.
(30) Makowski, A. J.; Patil, C. A.; Mahadevan-Jansen, A.; Nyman, J. S. Polarization control of Raman spectroscopy optimizes the assessment of bone tissue. *J. Biomed. Opt.* **2013**, *18*, 55005.
(31) Janko, M.; Davydovskaya, P.; Bauer, M.; Zink, A.; Stark, R. W. Anisotropic Raman scattering in collagen bundles. *Opt. Lett.* **2010**, *35*, 2765−2767.
(32) Hunziker, E. B.; Michel, M.; Studer, D. Ultrastructure of adult human articular cartilage matrix after cryotechnical processing. *Microsc. Res. Tech.* **1997**, *37*, 271−284.
(33) Matcher, S. J. What can biophotonics tell us about the 3D microstructure of articular cartilage? *Quant. Imaging Med. Surg.* **2015**, *5*, 143−158.
(34) Felten, J.; Hall, H.; Jaumot, J.; Tauler, R.; de Juan, A.; Gorzsas, A. Vibrational spectroscopic image analysis of biological material using multivariate curve resolution-alternating least squares (MCR-ALS). *Nat. Protoc.* **2015**, *10*, 217−240.
(35) Oyen, M. L.; Shean, T. A. V.; Strange, D. G. T.; Galli, M. Size effects in indentation of hydrated biological tissues. *J. Mater. Res.* **2012**, *27*, 245−255.
(36) Redler, I.; Mow, V. C.; Zimny, M. L.; Mansell, J. The ultrastructure and biomechanical significance of the tidemark of articular cartilage. *Clin. Orthop. Relat. Res.* **1975**, *112*, 357−362.
(37) Oyen, M. L. Mechanical characterisation of hydrogel materials. *Int. Mater. Rev.* **2014**, *59*, 44−59.
(38) Katz, J. L. Hard tissue as a composite material—I. Bounds on the elastic behavior. *J. Biomech.* **1971**, *4*, 455−473.
(39) Keeney, M.; Lai, J. H.; Yang, F. Recent progress in cartilage tissue engineering. *Curr. Opin. Biotechnol.* **2011**, *22*, 734−740.
(40) Klein, T. J.; Malda, J.; Sah, R. L.; Hutmacher, D. W. Tissue engineering of articular cartilage with biomimetic zones. *Tissue Eng., Part B* **2009**, *15*, 143−157.
(41) Kandel, R. A.; Chen, H.; Clark, J.; Renlund, R. Transplantation of cartilagenous tissue generated in vitro into articular joint defects. *Artif. Cells Blood Substit. Immobil. Biotechnol.* **1995**, *23*, 565−577.
(42) Hayes, A. J.; Hall, A.; Brown, L.; Tubo, R.; Caterson, B. Macromolecular organization and in vitro growth characteristics of scaffold-free neocartilage grafts. *J. Histochem. Cytochem.* **2007**, *55*, 853−866.
(43) St-Pierre, J. P.; Wang, Q.; Li, S. Q.; Pilliar, R. M.; Kandel, R. A. Inorganic polyphosphate stimulates cartilage tissue formation. *Tissue Eng., Part A* **2012**, *18*, 1282−1292.
(44) Lapadula, G.; Nico, B.; Cantatore, F. P.; La Canna, R.; Roncali, L.; Pipitone, V. Early ultrastructural changes of articular cartilage and synovial membrane in experimental vitamin A-induced osteoarthritis. *J. Rheumatol.* **1995**, *22*, 1913−1921.
(45) Suits, J. M.; Khan, A. A.; Waldman, S. D. Glycogen storage in tissue-engineered cartilage. *J. Tissue Eng. Regener. Med.* **2008**, *2*, 340−346.

DOI: 10.1021/acscentsci.6b00222
ACS Cent. Sci. 2016, 2, 885−895